

RESEARCH ARTICLE

Biological variation in the sizes, shapes and locations of visual cortical areas in the mouse

Jack Waters ^{*}, Eric Lee, Nathalie Gaudreault, Fiona Griffin, Jerome Lecoq, Cliff Slaughterbeck, David Sullivan, Colin Farrell, Jed Perkins, David Reid, David Feng, Nile Graddis, Marina Garrett, Yang Li, Fuhui Long, Chris Mochizuki, Kate Roll, Jun Zhuang , Carol Thompson

Allen Institute for Brain Science, Seattle, WA, United States of America

* jackw@alleninstitute.org



OPEN ACCESS

Citation: Waters J, Lee E, Gaudreault N, Griffin F, Lecoq J, Slaughterbeck C, et al. (2019) Biological variation in the sizes, shapes and locations of visual cortical areas in the mouse. PLoS ONE 14(5): e0213924. <https://doi.org/10.1371/journal.pone.0213924>

Editor: Nicholas V. Swindale, University of British Columbia, CANADA

Received: October 10, 2018

Accepted: March 4, 2019

Published: May 1, 2019

Copyright: © 2019 Waters et al. This is an open access article distributed under the terms of the [Creative Commons Attribution License](https://creativecommons.org/licenses/by/4.0/), which permits unrestricted use, distribution, and reproduction in any medium, provided the original author and source are credited.

Data Availability Statement: All relevant data are within the manuscript and its Supporting Information files.

Funding: We wish to thank the Allen Institute founder, Paul G. Allen, for his vision, encouragement and support. The funders had no role in study design, data collection and analysis, decision to publish, or preparation of the manuscript.

Competing interests: The authors have declared that no competing interests exist.

Abstract

Visual cortex is organized into discrete sub-regions or areas that are arranged into a hierarchy and serves different functions in the processing of visual information. In retinotopic maps of mouse cortex, there appear to be substantial mouse-to-mouse differences in visual area location, size and shape. Here we quantify the biological variation in the size, shape and locations of 11 visual areas in the mouse, after separating biological variation and measurement noise. We find that there is biological variation in the locations and sizes of visual areas.

Introduction

Mammalian neocortex is generally considered to be organized into discrete anatomically and functionally defined sub-regions or areas. For example, a major portion of posterior cortex is concerned primarily with vision and is divided into discrete visual areas, >20 areas in primates [1] and ~15 in the mouse [2]. Visual areas are arranged into a hierarchy and serve different functions in the processing of visual information [3] and yet the sizes and shapes of visual areas appear to vary across individuals of a given species. In mice for example, maps of visual cortex consist of a stereotyped collection of visual areas, in approximately the same relative locations in each mouse, but the relative positions of areas and in their sizes and shapes appear to differ substantially between mice. Such differences in the organization of cortex might affect the processing of visual information across mice. How much variation is there in the locations, sizes and shapes of cortical areas from mouse to mouse?

Only a few studies describe differences in the size, shape and locations of cortical areas across a population of individuals. Differences have been described in the size and shape of primary visual cortex in humans, macaques, cats, rats and mice, the consensus being that V1 differs in size more than in shape [4–7]. Necessarily, comparisons were across small numbers (<25) of individuals and no attempt was made to determine whether the differences resulted from differing organization of cortex across individuals (biological variation) or simply measurement error (noise). Separating biological variation from measurement noise requires statistical analysis of measurements from large numbers of animals. To our knowledge, nobody

has assessed biological variation (after separation from measurement noise) of any cortical area in any species.

In our previous work, we noted that retinotopic maps of cortical visual areas differed between mice [2], but did not quantify these differences or determine the relative contributions of biological variation and measurement noise. Here we quantify the variability in size, shape and locations of cortical visual areas in the mouse

Results and discussion

Retinotopic maps differ across mice (S1 Fig). The differences between maps presumably include biological variation and inaccuracies, or measurement noise in the mapping process. Under the assumption that the retinotopic map is invariant in an individual, repeated map generation from a mouse will result in maps that differ only because of measurement noise. This assumption provides a method to isolate biological variation, given maps from a large enough collection of mice and two or more maps from each mouse. From such a data set, one can estimate (1) the effects of measurement noise, by comparing retinotopic maps across mapping sessions in each mouse, and (2) the combined effects of biological variability and measurement noise, by comparing retinotopic maps across mice. A second assumption, that measurement noise and biological variation are independent, permits the isolation of biological variation by subtraction of the variance of the between-session comparisons from the variance of the between-mouse comparisons. Implicitly, a third assumption is made: that there are no additional sources of measurement noise when comparing maps across mice, relative to the comparison across mapping sessions.

We generated retinotopic maps for 60 adult mice by intrinsic signal imaging [8–10]. Each mouse was imaged twice, 11–121 days apart (Fig 1A). As in our previous publication [2], retinotopy was displayed using the visual field sign [7] and field sign maps were segmented into retinotopically-defined cortical areas using a numerical routine [2,11]. Maps were aligned to the 3D Allen Mouse Brain Reference Atlas, assisted by surface vasculature images acquired during mapping (S2 Fig).

The mean sign map included 11 visual areas (Fig 1B; V1, RL, LM, AM, PM, P, RLL, AL, LLA, MMA, MMP). Consistent with our previous paper [2], there was an almost continuous ring of field sign positive regions around V1 and the lateral retinotopic border of V1 was ~300 μm medial to the 3D Allen Mouse Brain Reference Atlas border (Fig 1C and 1D).

Biological variation in the locations of visual areas

To test for biological variation in the locations of visual areas, we compared maps across mice and across imaging sessions. We reduced each map to a set of points, each point representing the centroid of a field sign patch and made pairwise comparisons of maps. As a measure of the difference between each pair of maps, we calculated the paired patch distance (ppd; S3 Fig). From 60 mice, two imaging sessions per mouse, we made 60 pairwise comparisons across sessions (one per mouse) and $59 * 60 = 3540$ pairwise comparisons across mice. For each pair of maps, we defined paired patch distance as the mean of the distances between corresponding field sign patches:

$$\text{paired patch distance} = \sum_1^n \frac{((x_i - x_j)^2 + (y_i - y_j)^2)^{0.5}}{n}$$

where, x and y are the coordinates of the centroid of each field sign patch in $m-l$ and $a-p$ axes, subscripts i and j denote the two maps being compared, n is the number of field sign patches in both maps

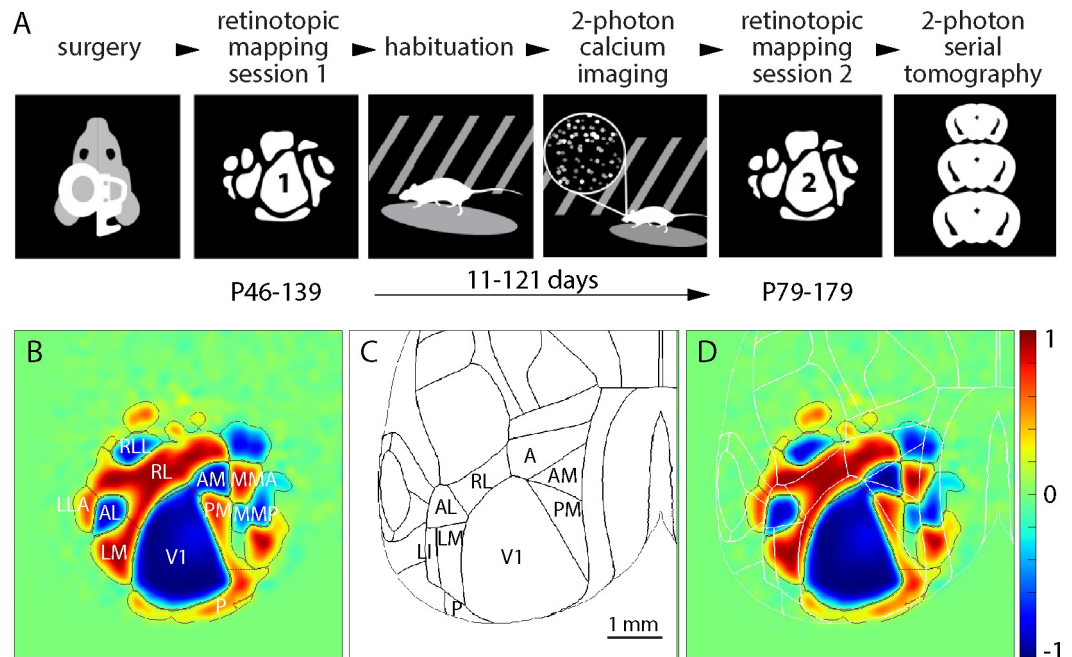


Fig 1. Repeated retinotopic mapping of mouse cortical areas. (A) Workflow of the Allen Brain Observatory, including implantation of a 5 mm diameter cranial window and retinotopic mapping at two time points, separated by 11–121 days. (B) Mean field sign map from 60 mice, with borders and labels for the 11 visual areas studied here. (C) Borders of cortical areas in the 3D Allen Mouse Brain Reference Atlas. Visual areas are labeled. (D) Mean sign map aligned to the 3D Allen Mouse Brain Reference Atlas, with atlas borders in white. The color scale bar applies to all field sign maps throughout the paper.

<https://doi.org/10.1371/journal.pone.0213924.g001>

There was no correlation between the time between imaging sessions and session-to-session ppd, consistent with maps being stable between imaging sessions (S1 Fig, panel B). Mouse-to-mouse and session-to-session distributions were significantly different ($p = 4.6 \times 10^{-9}$, Mann-Whitney U test), with mouse-to-mouse differences being greater than session-to-session differences. We conclude that there is biological variation in the retinotopic map.

For each pairwise comparison of maps, one map could be translated relative to the other, or rotated, scaled or the relative locations of visual areas might differ. Any combination of these four transformations might be the source of the observed biological variability. In addition, inaccuracies in our alignment process might generate translation and rotation errors that differ between mouse-to-mouse and session-to-session comparisons and therefore be interpreted, erroneously, as biological variation. To separate differences in translation, rotation, scale and shape (shape, in this context, is the relative locations of patches), we adopted Procrustes superimposition, an analytical approach used to compare shapes in biological populations [12–14]. The approach involves the sequential estimation and removal of translation, rotation and scaling to leave differences in only the locations of patches.

Across maps, the centroid of V1 moved by up to 1 mm in m-l and a-p axes. As might be expected, the distributions of mouse-to-mouse and session-to-session differences were different for V1 centroid locations in both a-p and m-l axes ($p = 9.0 \times 10^{-6}$ and 5.1×10^{-12} respectively, Levene's test, Fig 2A and 2B). As a measure of the scale of each retinotopic map we calculated a statistic we call the 'centroid size' from the centroids of areas V1, RL and PM, all three of which were in every field sign map. Centroid size is the square root of the summed squared distances of each landmark from the centroid [14]. Mean centroid size was 1.46 mm, with centroid sizes being approximately normally distributed about this mean, most within

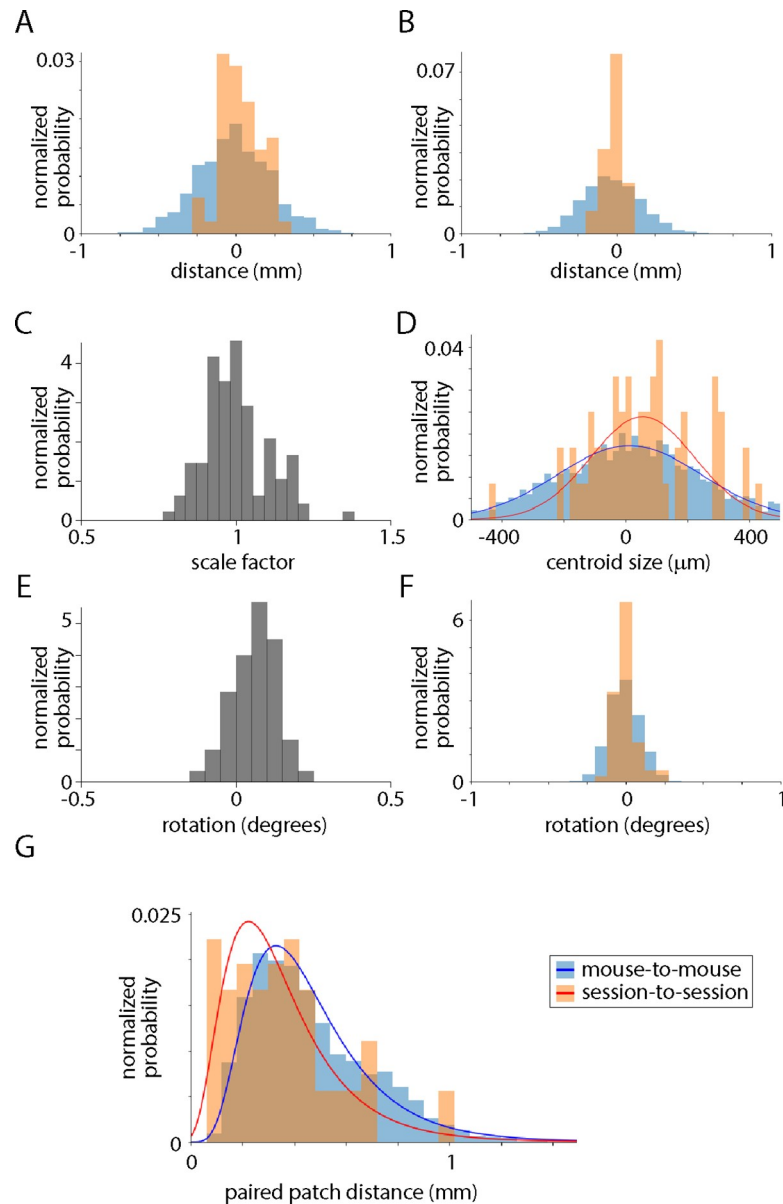


Fig 2. Location, scaling and rotation of maps. (A) Frequency histogram of V1 centroid positions for 3540 pairwise mouse-to-mouse comparisons and 60 pairwise session-to-session comparisons. Distance is in the a-p axis with higher numbers corresponding to more posterior locations. (B) Frequency histogram of V1 centroid positions for 3540 pairwise mouse-to-mouse comparisons and 60 pairwise session-to-session comparisons. Distance is in the m-l axis with higher numbers corresponding to more medial locations. (C) Distribution of scale factors applied to maps, where scale factor is calculated as the centroid size of the map divided by that derived from the mean field sign map. (D) Frequency histogram of centroid size differences for 3540 pairwise mouse-to-mouse comparisons and 60 pairwise session-to-session comparisons. (E) Distribution of rotations applied to maps during alignment. (F) Frequency histogram of rotations for 3540 pairwise mouse-to-mouse comparisons and 60 pairwise session-to-session comparisons. (G) Frequency histogram of inter-patch distances for 3540 pairwise mouse-to-mouse comparisons and 60 pairwise session-to-session comparisons, after elimination of translation, scale and rotation differences between maps. Frequency is displayed as a fractional probability, the integral of each distribution being 1. Lines are lognormal fits.

<https://doi.org/10.1371/journal.pone.0213924.g002>

~20% of the mean (Fig 2C). The mouse-to-mouse distribution of centroid sizes was broader than the session-to-session distribution ($p = 0.0026$, Levene's test, Fig 2D), indicating that

there was biological variation in the size of the visual map. Rotations were extremely small (range -0.11 to 0.22 degrees, Fig 2E) and mouse-to-mouse and session-to-session differences in rotation were similar (Fig 2F). We aligned maps, eliminating differences in location, scale and rotation. Comparing across the population of maps, neither map shape nor the area of V1 displayed obvious dependence on the scaling applied to the map during alignment (S1 Fig, panel D, E). After eliminating differences in location, scale and rotation, and re-tested for biological variation, finding that a significant difference between the distributions remained ($p = 4.4 \times 10^{-5}$, Mann-Whitney U test; Fig 2G). We conclude that there is biological variation in the overall shape of the retinotopic map in the mouse, in other words, that the field sign patches are in different locations in different mice.

We further quantified the differences in centroid location for each field sign patch, aiming to calculate the biological variation in location for each patch. Our approach is similar to that of Garrett *et al.* [7], but here we separate biological variation and measurement noise. Mouse-to-mouse differences in centroid location were greater than session-to-session differences for all 11 patches and in both a-p and m-l axes (Fig 3A and 3B), permitting us to estimate biological variation by subtraction of variances. For most patches, biological variation and measurement noise were approximately equal contributors to mouse-to-mouse differences in the visual area map (Fig 3B). The standard deviation of biological variation was $\sim 200 \mu\text{m}$ for many patches or $\sim 15\%$ of the diameter of the mean patch (Fig 3C).

Size and shape of each field sign patch

When comparing retinotopic maps from different mice, there appears to be striking variation in the sizes and shapes of most patches in the map (S1 Fig). We further explored biological variation in the size and shape of each field sign patch, to determine whether there is biological variation and to quantify it.

We began by comparing mouse-to-mouse and session-to-session differences in the area of each field sign patch (Fig 4A). For 9 of 11 patches, the variance of the mouse-to-mouse distribution was greater than the variance of the session-to-session differences. Fig 4B plots biological variation for these 9 patches and measurements noise for all 11 patches. The distributions were significantly different for V1, which was also the patch with the least biological variation in size, with a standard deviation of 16%. Hence in 50% of mice, V1 is $>11\%$ smaller or larger than average and in 5% of mice, V1 is $>32\%$ smaller or larger than average. For the other patches, mouse-to-mouse distributions were not significantly different from session-to-session differences (each $p > 0.05/11$, Levene's test with Bonferroni correction) and we can be less confident that there was biological variation in the sizes of the other patches, but the fact that the variance of the mouse-to-mouse distribution was greater than the variance of the session-to-session differences for almost all the patches suggests that there's biological variation in size for many of them. Although measurement noise was the main source of variability in patch size, biological variation was also substantial at 16–56% of the area of the mean patch (Fig 4C). The mean standard deviation of biological variation across all patches was 32%. Hence in 50% of mice, the mean patch is $>22\%$ smaller or larger than average and in 5% of mice, the mean patch is $>64\%$ smaller or larger than average. There was no correlation between the area of V1 and the age (Fig 4D) or weight (Fig 4E) of the mouse and the areas and locations of patches differed little with sex or Cre line (Fig 4G, S4 Fig). There was no correlation between the sizes of patches across mice ($p < 0.05/11$, Spearman rank-order correlation), so the sizes of neighboring patches are unrelated.

We investigated biological variation in the shapes of field sign patches using the Jaccard index, defined as the area of intersection of two patches divided by the area of their union.

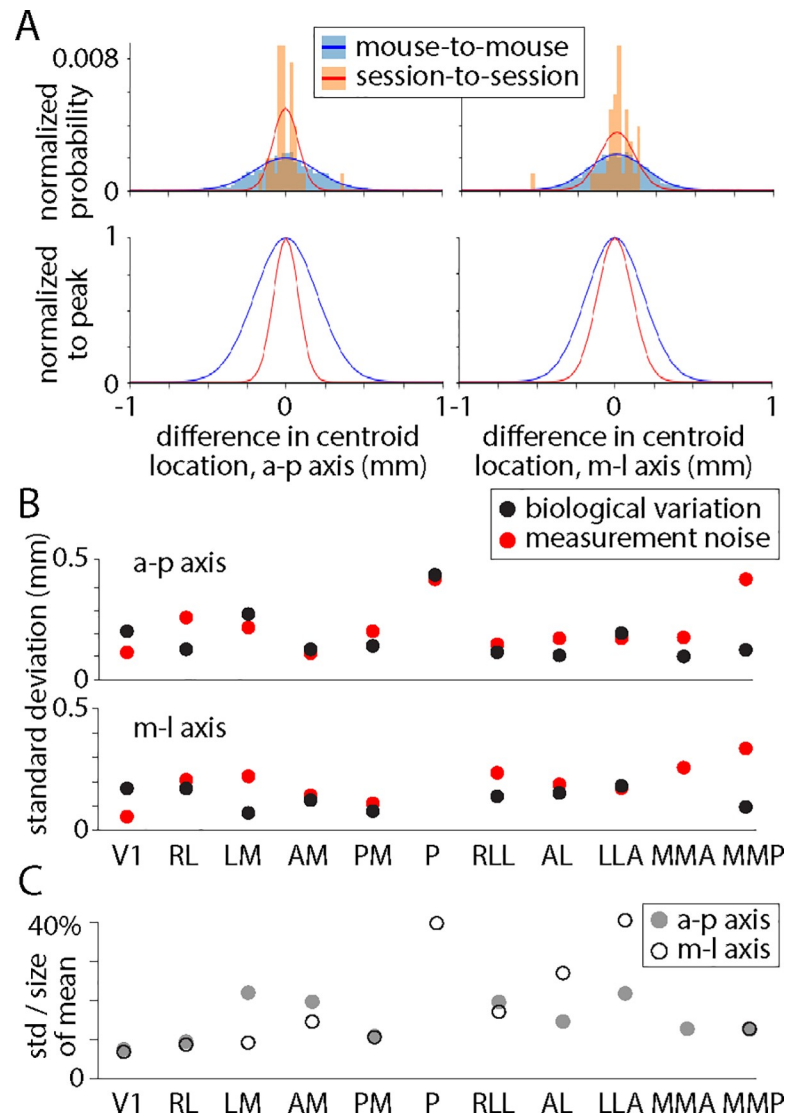


Fig 3. Biological variation in the locations of field sign patches. (A) Frequency histograms illustrating mouse-to-mouse and session-to-session differences in centroid location for AM. Frequency is displayed as a normalized probability, the integral of each distribution being 1. Lines are fits to a normal distribution. Below: same distributions normalized to their peaks. (B) Standard deviations of biological variation and measurement noise for distributions of differences in centroid location. (C) Standard deviation of the biological variation of centroid positions, in a-p and m-l axes, expressed as a percentage of the maximum width of the mean of each patch.

<https://doi.org/10.1371/journal.pone.0213924.g003>

Jaccard index ranges from 0 (no overlap) to 1 (identical shapes). We calculated differences pairwise for mouse-to-mouse and for session-to-session comparisons, resulting in mouse-to-mouse and session-to-session distributions of the Jaccard index for each patch. The median Jaccard indices of mouse-to-mouse and session-to-session distributions were similar for all patches (Fig 5A) and there was no patch for which the means of the two distributions differed significantly (each $p > 0.05 / 11$, Mann-Whitney U test with Bonferroni correction). Consistent with this conclusion, plots of the cumulative mouse-to-mouse and session-to-session differences were similar (V1 in Fig 5B), with no indication that mouse-to-mouse differences were greater than session-to-session differences in patch shape. Hence we find no evidence for biological variation in the shapes of visual areas, the apparent variability across mice resulting

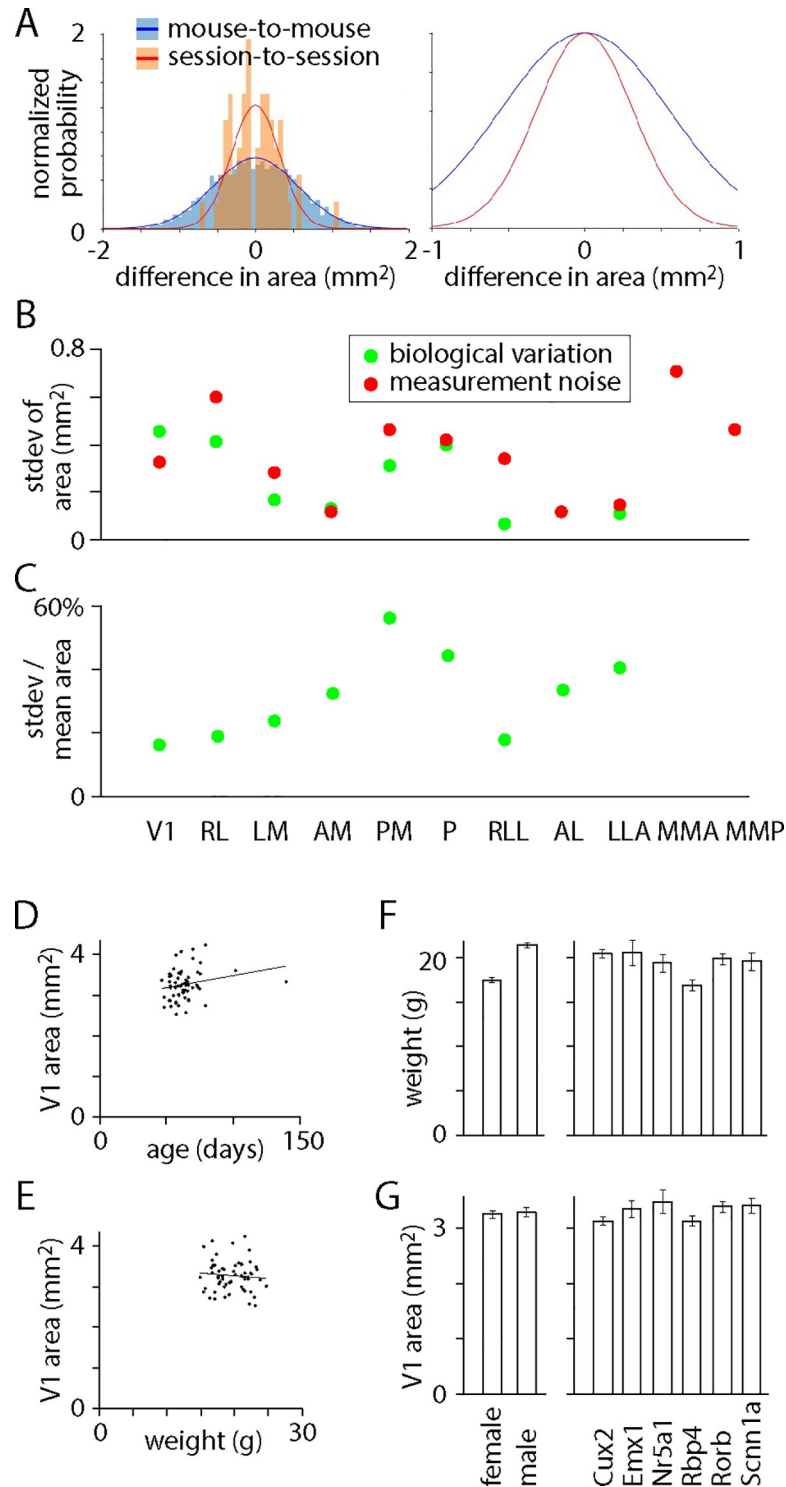


Fig 4. Biological variation in the sizes of field sign patches. (A) Histogram of mouse-to-mouse and session-to-session differences in area of V1. Frequency is displayed as a fractional probability, the integral of each distribution being 1. Lines are normal distributions. Right: same distributions normalized to their peaks. (B) Standard deviations of biological variation and measurement noise for distributions of differences in area. (C) For each patch, standard deviation of biological variation in patch area as a percentage of the area of the mean patch. (D) Area of V1 in the first imaging session, as a function of postnatal age during the first imaging session. Line is a linear fit. (E) Area of V1 in the first imaging session, as a function of weight during the first imaging session. Line is a linear fit. (F) Weights of mice at

first imaging session, sorted by sex (left) and Cre line (right). Mean \pm SEM. (G) V1 area in first imaging session, sorted by sex (left) and Cre line (right). Mean \pm SEM.

<https://doi.org/10.1371/journal.pone.0213924.g004>

from measurement noise. This result makes a strong statement about the reliability of border positions in maps based on intrinsic imaging. The reproducibility of these maps is poor, even with extensive averaging, likely because the signal-to-noise ratio of intrinsic imaging is low. One might interpret the resulting border positions as approximate. In contrast, border locations mapped with GCaMP6 indicators, an approach which can offer a higher signal-to-noise ratio than intrinsic imaging, can be accurate to within tens of micrometers [2].

We have assumed that biological variation is the only difference between mouse-to-mouse and session-to-session comparisons. Might some other mouse-to-mouse difference have been classified as biological variation? Alignment errors are a concern, but our results show no evidence of such alignment effects and the resulting errors would likely affect the locations of visual areas and have little effect on their sizes. Hence alignment errors are unlikely to account for the observed biological variation in the sizes of visual areas. Mouse-to-mouse differences in the segmentation of field sign patches, arising from differences in the signal-to-noise ratio of the underlying images, might contribute to the biological variation in size of patches. We expect the effect to be greater for peripheral patches (patch P, for example) than for V1 and other patches near the core of the map.

In summary, we assessed biological variation in the sizes, shapes and locations of field sign patches in visual cortex of the mouse. Our results provide no evidence for biological variation

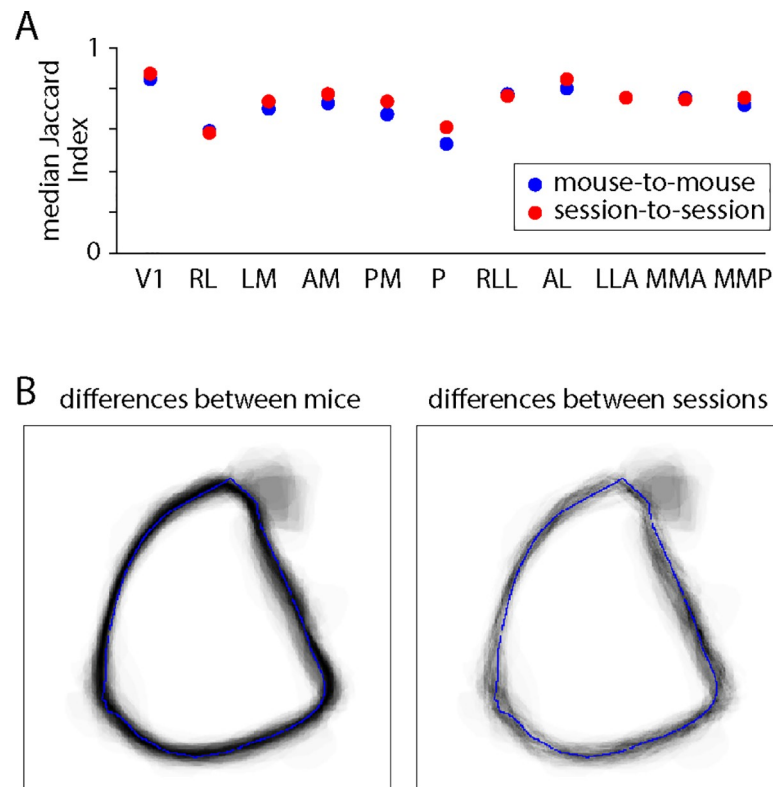


Fig 5. Biological variation in the shapes of field sign patches. (A) Median of the distribution of the Jaccard Indices for mouse-to-mouse and session-to-session comparisons, for each patch. (B) Cumulative differences in V1 for mouse-to-mouse and session-to-session pairwise comparisons.

<https://doi.org/10.1371/journal.pone.0213924.g005>

in the shapes of visual areas and evidence of only modest biological variation in location, but the sizes of visual areas differed substantially between mice, with the area of the average region varying ~2-fold across the population of mice. We were surprised by this result. We reasoned that there is some minimum amount of cortical tissue required for each visual area to perform its functions and likely sufficient, but not excess cortex is allocated to each visual area. If the functions of each visual area are invariant across mice, it seems likely that the required volume of cortex for each visual area is similar across mice. Hence our expectation was that there might be variability in the locations and shapes of visual areas, but that size would be more constrained. Our results are not consistent with this expectation, raising the possibility the roles of visual areas in the processing of visual information is more flexible than we had appreciated.

Materials and methods

Mouse lines

Retinotopic maps were generated from 60 mice of 7 genotypes: 20 Cux2-CreERT2;Camk2a-tTA;Ai93 mice, 5 Emx1-IRES-Cre;Camk2a-tTA;Ai93 mice, 1 Emx1-IRES-Cre;Camk2a-tTA;Ai94 mouse, 7 Nr5a1-Cre;Camk2a-tTA;Ai93 mice, 10 Rbp4-Cre;Camk2a-tTA;Ai93 mice, 11 Rorb-IRES2-Cre;Camk2a-tTA;Ai93 mice and 6 Scnn1a-Tg3-Cre;Camk2a-tTA;Ai93 mice.

Mice were crosses of the following lines:

Cux2-CreERT2 [15] https://www.mmrrc.org/catalog/sds.php?mmrrc_id=32779).

Emx1-IRES-Cre: B6.129S2-Emx1tm1(crc)Krl/J [16] <https://www.jax.org/strain/005628>)

Nr5a1-Cre [17] https://www.mmrrc.org/catalog/sds.php?mmrrc_id=34276

Rbp4-Cre_KL100 [18] https://www.mmrrc.org/catalog/sds.php?mmrrc_id=31125

Rorb-IRES2-Cre [19,20] <https://www.jax.org/strain/023526>

Scnn1a-Tg3-Cre [21] <https://www.jax.org/strain/009613>

CaMK2a-tTA: B6.Cg-Tg(Camk2a-tTA)1Mmay/DboJ [22] <https://www.jax.org/strain/007004>

Ai93: B6;129S6-Igs7^{tm93.1(tetO-GCaMP6f)Hze}/J [23] <https://www.jax.org/strain/024103>

Ai94: B6.Cg-Igs7^{tm94.1(tetO-GCaMP6s)Hze}/J [23] <https://www.jax.org/strain/024104>

Retinotopic mapping and identification of visual areas

All animal procedures were approved by the Institutional Animal Care and Use Committee of the Allen Institute for Brain Science. Retinotopic maps were generated by intrinsic signal imaging as part of the Allen Brain Observatory data product (<http://observatory.brain-map.org/visualcoding/>) and imaging methods are described in the Allen Brain Observatory literature (http://help.brain-map.org/display/observatory/Documentation?preview=/10616846/10813483/VisualCoding_Overview.pdf). Retinotopic mapping was performed under isoflurane anesthesia (1–1.4%, inhaled). Altitude and azimuth maps were converted to a field sign map and the borders between areas were identified using code presented in our previous paper [2]. Here we took the additional step of automating the identification of 11 visual areas.

The field sign is defined as the sine of the difference in angle between altitude and azimuth gradients. Field sign was calculated pixelwise, yielding a field sign map. Visual areas appear on the field sign map as regions of consistent field sign (positive or negative) and the field sign passes through zero at borders between visual areas.

Alignment of maps

Maps were aligned across mice and imaging sessions. Images from the first imaging session were aligned to the 3D Allen Mouse Brain Reference Atlas as described previously [24] (<http://>

help.brain-map.org/display/mouseconnectivity/Documentation?preview=/2818171/10813534/Mouse_Common_Coordinate_Framework.pdf). The origin of the reference space is an arbitrary point anterior, ventral and lateral (left) of the brain. The mean location of V1 was 9.14 mm posterior and 3.01 mm medial from the origin of the reference space. Images from the second imaging session were aligned to the first session using the surface vasculature images and a scale-invariant feature transform algorithm implemented in opencv.

Translation, scaling and rotation of maps

In Procrustean morphometrics, shape is what remains after the removal of differences in translation, scale (or size) and rotation [12–14]. To compare the shapes of retinotopic maps, we used a Procrustean approach, eliminating map-to-map differences in translation, scale and rotation. We converted each map into a collection of centroids, one for each field sign patch. We translated maps such that the centroid of V1 was at the origin. We normalized the size of each map using the centroids of patches V1, RL and PM since these three patches were identified in every map. These three centroids form a triangle and we scaled each map such that the circumference of this triangle equaled one. Finally, we rotated each map about the origin (the centroid of V1) to minimize the sum of distances between the centroids of corresponding patches (RL in map 1 vs RL in map 2, LM vs LM, etc.).

Data sets and analysis code

We include two Jupyter notebooks with this manuscript. The ‘data viewer’ notebook provides code to download and view the data sets. The ‘analysis’ notebook contains most of the plots and analyses in the manuscript and some additional analyses.

Supporting information

S1 Fig. Field sign maps from 60 mice. (A) Field sign maps from the first imaging session for each of 60 mice, to illustrate the mouse-to-mouse variability in field sign maps. (B) Plot of paired patch distance (ppd) as a function of time between first and second imaging sessions. Line: best linear fit, slope -0.08. (C) Histogram of the number of times each patch appeared in retinotopic maps. Each patch could occur in a maximum of 60 maps (one for each of 60 mice) for each of the first and second imaging sessions. The right column indicates the number of mice in which the patch was visible in both imaging sessions. (D) Relationship between the scale factor applied to each map and its shape. Shape was measured as the ppd of the map in pairwise comparison with the mean sign map (from 60 mice). Each point represents one map from session 1. (E) Relationship between the scale factor applied to each map and its relative V1 area, where relative V1 area is V1 area in the map divided by the area of V1 in the mean sign map. Each point represents one map from session 1. (TIF)

S2 Fig. Schematic of analysis workflow. Schematic illustration of the sequence of steps in the core of the analysis. (TIF)

S3 Fig. Illustration of paired patch distance. (A) Field sign maps from two mice. For each map, the postnatal age (in days) during imaging is provided. Comparison across mice (across rows) describes the sum of biological variation and measurement noise. Comparison across imaging sessions (down columns) describes measurement noise. The difference between the two comparisons provides an estimate of biological variation. (B) Maps of centroid locations for each field sign patch in mouse 1. Each centroid is colored to match the field sign of its

parent field sign patch. (C) Comparison of two maps, with the distances between patches illustrated with black lines. The paired patch distance (ppd) is the mean of these distances.

(TIF)

S4 Fig. Patch locations and surface areas, by Cre line. Centroid positions (a-p axis, left column; m-l axis, central column) and surface area (right column) for each patch, sorted by Cre line. No significant differences between Cre lines in any plot (ANOVA, $p > 0.05$).

(TIF)

S1 Codeipynb. Jupyter notebook with code to download and view data sets.

(IPYNB)

S2 Codehtml. HTML copy of notebook_data_viewer.ipynb.

(HTML)

S3 Codeipynb. Jupyter notebook containing analysis of data sets.

(IPYNB)

S4 Codehtml. HTML copy of notebook_analysis.ipynb.

(HTML)

Acknowledgments

We wish to thank the Allen Institute founder, Paul G. Allen, for his vision, encouragement and support.

Author Contributions

Conceptualization: Jack Waters.

Data curation: Jack Waters.

Formal analysis: Jack Waters.

Investigation: Eric Lee, Nathalie Gaudreault, Fiona Griffin, Kate Roll.

Methodology: Cliff Slaughterbeck, David Sullivan, Colin Farrell, David Reid.

Software: Jack Waters, Jed Perkins, David Feng, Nile Graddis, Yang Li, Fuhui Long, Chris Mochizuki.

Validation: Jack Waters.

Visualization: Jack Waters.

Writing – original draft: Jack Waters.

Writing – review & editing: Jack Waters, Eric Lee, Nathalie Gaudreault, Fiona Griffin, Jerome Lecoq, Cliff Slaughterbeck, David Sullivan, Colin Farrell, Jed Perkins, David Reid, David Feng, Nile Graddis, Marina Garrett, Yang Li, Fuhui Long, Chris Mochizuki, Kate Roll, Jun Zhuang, Carol Thompson.

References

1. Gattass R, Nascimento-Silva S, Soares JGM, Lima B, Jansen AK, Diogo ACM, Farias MF, Marcondes M, Botelho EP, Mariani OS, Azzi J, Fiorani M (2005) Cortical visual areas in monkeys: location, topography, connections, columns, plasticity and cortical dynamics. *Phil Trans R Soc B: Biological Sciences* 360, 709–731. <https://doi.org/10.1098/rstb.2005.1629> PMID: 15937009

2. Zhuang J, Ng L, Williams D, Valley M, Li Y, Garrett M, Waters J (2017) An extended retinotopic map of mouse cortex. *eLife* 6, e18372. <https://doi.org/10.7554/eLife.18372> PMID: 28059700.
3. Van Essen DC, Maunsell JHR (1983) Hierarchical organization and functional streams in the visual cortex. *Trends Neurosci* 6, 370–375.
4. Van Essen DC, Newsome WT, Maunsell JHR (1984) *Vision Research* 24, 449–428.
5. Duffy KR, Murphy KM, Jones DG (1998) Analysis of the postnatal growth of visual cortex. *Visual Neuroscience* 15, 831–839. PMID: 9764525
6. Hinds O, Polemi JR, Rajendran N, Balasubramanian M, Wald LL, Augustinack JC, Wiggins G, Rosas HD, Fischl B, Schwartz EL (2008) *Cerebral Cortex* 18, 2586–2595. <https://doi.org/10.1093/cercor/bhn016>
7. Garrett ME, Nauhaus I, Marshel JH, Callaway EM (2014) Topography and areal organization of mouse visual cortex. *J Neurosci* 34, 12587–12600. <https://doi.org/10.1523/JNEUROSCI.1124-14.2014> PMID: 25209296
8. Schuett S, Bonhoeffer T, Hübener M (2002) Mapping retinotopic structure in mouse visual cortex with optical imaging. *J Neurosci* 22(15), 6549–6559. PMID: 12151534
9. Kalatsky VA, Stryker MP (2003) New paradigm for optical imaging: temporally encoded maps of intrinsic signal. *Neuron* 38, 529–545. PMID: 12765606
10. Marshel JH, Garrett ME, Nauhaus I, Callaway EM (2011) Functional specialization of seven mouse visual cortical areas. *Neuron* 72(6), 1040–1054. <https://doi.org/10.1016/j.neuron.2011.12.004> PMID: 22196338
11. Juavinett AL, Nauhaus I, Garrett ME, Zhuang J, Callaway EM (2017) Automated identification of mouse visual areas with intrinsic signal imaging. *Nature Protocol* 12, 32–43.
12. Goodall C (1991) Procrustes methods in the statistical analysis of shape. *Journal of the Royal Statistical Society Series B* 53, 285–339.
13. Webster M, Sheets HD (2010) An introduction to landmark-based geometric morphometrics. In: *The Paleontological Society Papers*, Vol. 16, Quantitative Methods in Paleobiology, pp. 163–188. Ed: Alroy J, Hunt G.
14. Zelditch ML, Swiderski DL, Sheets HD (2012) *Geometric Morphometrics for Biologists*. Pub. Academic Press. ISBN 978-0-12-386903-6.
15. Franco SJ, Gil-Sanz C, Martinez-Garay I, Espinosa A, Harkins-Perry SR, Ramos C, Müller U (2012) Fate-restricted neural progenitors in the mammalian cerebral cortex. *Science* 337, 746–749. <https://doi.org/10.1126/science.1223616> PMID: 22879516
16. Gorski JA, Talley T, Qiu M, Puelles L, Rubenstein JL, Jones KR (2002) Cortical excitatory neurons and glia, but not GABAergic neurons, are produced in the Emx1-expressing lineage. *J Neurosci* 22, PMID: 12151506
17. Dhillon H, Zigman JM, Ye C, Lee CE, McGovern RA, Tang V, Kenny CD, Christiansen LM, White RD, Edelstein EA, Coppari R, Balthasar N, Cowley MA, Chua S Jr, Elmquist JK, Lowell BB (2006) Leptin directly activates SF1 neurons in the VMH, and this action by leptin is required for normal body-weight homeostasis. *Neuron* 49, 191–203. <https://doi.org/10.1016/j.neuron.2005.12.021> PMID: 16423694
18. Gong S, Doughty M, Harbaugh CR, Cummins A, Hatten ME, Heintz N, Gerfen CR (2007) Targeting Cre recombinase to specific neuron populations with bacterial artificial chromosome constructs. *J Neurosci* 27, 9817–9823. <https://doi.org/10.1523/JNEUROSCI.2707-07.2007> PMID: 17855595
19. Oh SW, Harris JA, Ng L, Winslow B, Cain N, Mihalas S, et al. (2014) A mesoscale connectome of the mouse brain. *Nature* 508, 207–214. <https://doi.org/10.1038/nature13186> PMID: 24695228
20. Harris JA, Hirokawa KE, Sorensen SA, Gu H, Mills M, Ng LL, Bohn P, Mortrud M, Ouellette B, Kidney J, Smith KA, Dang C, Sunkin S, Bernard A, Oh SW, Madisen L, Zeng H (2014) Anatomical characterization of Cre driver mice for neural circuit mapping and manipulation. *Front Neural Circuits* 8, 76. <https://doi.org/10.3389/fncir.2014.00076> PMID: 25071457
21. Madisen L, Zwingman TA, Sunkin SM, Oh SW, Zariwala HA, Gu H, Ng LL, Palmiter RD, Hawrylycz MJ, Jones AR, Lein ES, Zeng H (2010) A robust and high-throughput Cre reporting and characterization system for the whole mouse brain. *Nat Neurosci* 13, 133–140. <https://doi.org/10.1038/nn.2467> PMID: 20023653
22. Mayford M, Bach ME, Huang YY, Wang L, Hawkins RD, Kandel ER (1996) Control of memory formation through regulated expression of a CaMKII transgene. *Science* 274, 1678–1683. PMID: 8939850
23. Madisen L, Garner AR, Shimaoka D, Chuong AS, Klapoetke NC, Li L, van der Bourg A, Niino Y, Egolf L, Monetti C, Gu H, Mills M, Cheng A, Tasic B, Nguyen TN, Sunkin SM, Benucci A, Nagy A, Miyawaki A, Helmchen F, Empson RM, Knöpfel T, Boyden ES, Reid RC, Carandini M, Zeng H (2015) Transgenic mice for intersectional targeting of neural sensors and effectors with high specificity and performance. *Neuron* 85, 942–958. <https://doi.org/10.1016/j.neuron.2015.02.022> PMID: 25741722

24. Kuan L, Li Y, Lau C, Feng D, Bernard A, Sunkin SM, Zeng H, Dang C, Hawrylycz M, Ng L, Li Y LC (2015) Neuroinformatics of the Allen Mouse Brain Connectivity Atlas. *Methods* 73, 4–17. <https://doi.org/10.1016/j.ymeth.2014.12.013> PMID: 25536338